Applied Catalysis B: Environmental 111–112 (2012) 492–501

Contents lists available at SciVerse ScienceDirect

Applied Catalysis B: Environmental

journal homepage: www.elsevier.com/locate/apcatb

Preparation of meso-macroporous carbon nanotube-alumina composite monoliths and their application to the preferential oxidation of CO in hydrogen-rich gases

Suhong Lu, Yuan Liu*

Tianjin Key Laboratory of Applied Catalysis Science and Engineering, Department of Catalysis Science and Technology, School of Chemical Engineering, Tianjin University, Tianjin 300072, China

ARTICLE INFO

Article history:
Received 7 August 2011
Received in revised form 26 October 2011
Accepted 1 November 2011
Available online 7 November 2011

Keywords:
Carbon nanotube
Alumina
Composite
Monolith
Preferential oxidation

ABSTRACT

A series of carbon nanotube (CNT)-alumina composite monoliths with meso-macroporous structures were successfully synthesized by imbibing macroporous monolithic polystyrene foams with carbon nanotube-alumina hydrosols. These composite monoliths possessed interconnected spherical macropores that mainly ranged in 10–40 μm and adjustable mesopores of several nanometers. CNTs were uniformly dispersed throughout the alumina matrix. The CNT content and the calcination temperature markedly influenced the mesoporous structure, mechanical strength and thermal conductivity of the composite monoliths, but they did not significantly influence the phase transitions of alumina. The Pt-Ni/CNT-Al_2O_3 monoliths that were calcined at 1300 °C exhibited high activity and selectivity with small Pt loading of 0.75 wt.% for the preferential oxidation of CO. The residual concentration of CO was purified to less than 100 ppm in the temperature range of 120–180 °C in CO_2 and water-containing hydrogen-rich gases at a volume space velocity of 10,400 h^{-1}. This type of composite monolith could potentially be used as a catalyst support for many different reactions.

1. Introduction

The preferential oxidation (PROX) of CO in hydrogen-rich gases is considered to be a simple and cost-effective approach to purifying CO for proton exchange membrane fuel cells (PEMFCs) [1]. The H_2-rich gases resulting from the catalytic reforming of hydrocarbons, which is typically followed by the water–gas shift reaction, contain 0.5–1.0 vol.% of CO. This level of CO must be decreased to less than 100 ppm to avoid electrode poisoning in the PEMFCs. Among the catalysts for CO-PROX, Pt-based catalysts [2], especially nickel- or cobalt-promoted platinum catalysts [3,4], are promising candidates. Conventional supports include CeO_2 [5], Al_2O_3 [6–8], SiO_2 [9], zeolite [10], and activated carbon [11]. The use of carbon nanotubes as a catalyst support has also been investigated [12,13], owing to their special structure, high mechanical strength, unique electronic properties and high thermal conductivity.

Recently, mesoporous and macroporous metal oxide materials have been the focus of widespread research for use in the fields of catalysis, separation, sensors, optics, and electronics [14–17]. With regard to their potential use as catalyst supports, their interconnected macropores can efficiently transfer reactant species, and their mesopores provide high surface area. However, drawbacks include the relatively poor mechanical and thermal conductivities of oxide materials. If used as a catalyst support, the inferior thermal conductivity could lead to the formation of hotspots on the catalyst surface, which would induce the deactivation of the catalyst via active component sintering or the formation of byproducts through side reactions. The addition of CNTs to meso-macroporous oxides could be a possible approach to improve the mechanical and thermal conductivities of pure meso-macroporous oxides.

A composite of CNTs with meso-macroporous oxides should possess properties of both CNTs and meso-macroporous oxides, including high surface area, reasonable mass transfer, high thermal and electrical conductivity, and good mechanical strength. In addition, based on the differences in properties of the CNTs and the metal oxides, bi-functional materials could potentially be designed. Furthermore, the construction of a composite with a monolithic structure could lead to convenient and flexible applications. However, to the best of our knowledge, only one report describing this type of composite can be found. Worsley et al. [18] have fabricated a series of SWNT-CA (single-wall CNT-based carbon aerogel)/oxide (SiO_2, SnO_2, TiO_2) composites by depositing oxides onto the nanoligament surfaces of SWNT-CA monoliths. Their study concentrated on the electrical conductivity and mechanical properties of these composites.

Alumina is an oxide that is widely used as a catalyst support, adsorption material, ceramic material, and among others [7,19]. Studies focusing on mesoporous and meso-macroporous alumina

* Corresponding author. Tel.: +86 022 87401675.
E-mail address: yuanliu@tju.edu.cn (Y. Liu).

0926-3373/$ – see front matter © 2011 Elsevier B.V. All rights reserved.
doi:10.1016/j.apcatb.2011.11.001

have recently been attractive areas of interest [20–22]. Therefore, a study on the preparation of meso-macroporous CNT-Al_2O_3 composite monoliths should be a valuable and interesting contribution. Previously we found that CNTs supported Pt-Ni catalyst exhibited high activity and selectivity for CO-PROX [23]. Therefore, meso-macroporous CNT-Al_2O_3 composite monolith supported Pt-Ni may be a potential better alternative for CO-PROX.

In this work, meso-macroporous CNT-Al_2O_3 composite monoliths were prepared, characterized and used as a support for a CO-PROX catalyst. A simple preparation method involving a polystyrene foam template was used, and the influences of CNT content and calcination temperature on the properties of the composite monoliths were investigated. The prepared Pt-Ni/CNT-Al_2O_3-1300-M exhibited excellent catalytic performance for CO-PROX. The preparation approach described here provides a practical and simple method to synthesize porous, monolithic CNT-oxide composites, and the results suggest that this type of material possesses tremendous potential for future applications.

2. Experimental

2.1. Preparation of meso-macroporous carbon nanotube-alumina composite monoliths

The macroporous monolithic polystyrene (PS) foams were prepared using a method that was similar to one previously reported by our group [24]. The meso-macroporous carbon nanotube-alumina composite monoliths were synthesized by imbibing macroporous monolithic polystyrene foams with carbon nanotube-alumina hydrosols. Prior to use, the as-received aligned multi-walled carbon nanotubes (CNTs, 10–20 nm i.d. and 5–15 μm length) were oxidized with an H_2SO_4–HNO_3 mixture to increase their hydrophilicity, as previously described [23]. The resulting carbon nanotubes were denoted as CNTs-OX.

The carbon nanotube-alumina hydrosols were prepared as follows: 4 g of pseudo-boehmite was added into 30 mL of distilled water, followed by vigorous stirring at room temperature for 1 h. Then 6.8 mL of HNO_3 (2 mol L^{-1}) was added dropwise into the above suspension to form translucent alumina hydrosols. After stirring for 10 min, 30 mL of CNTs-OX that had been dispersed by ultrasonic agitation in distilled water was added to the alumina hydrosols. The mixture was allowed to continue stirring for 5 h.

Afterward, the PS foams were completely immersed in the carbon nanotube-alumina hydrosols under modest vacuum until no air escaped from the PS foams. Then the infused PS foams were transferred to a 60 °C drying oven for 12 h. The imbibing and drying procedures were repeated several times.

All composite monoliths were calcined at 600 °C for 4 h with a heating rate of 1 °C min^{-1} under a stream of N_2 (30 mL min^{-1}). Some samples were further calcined under a stream of N_2 at 900, 1100 or 1300 °C for 2 h.

The meso-macroporous CNT-alumina composite monoliths were labeled as *x* wt.% CNT-Al_2O_3-*y*-M, where *x* is the CNT to Al_2O_3 weight ratio, which was 0.5, 1.0, 3.0, 5.0, or 15.0, *y* is the calcination temperature, which was 600, 900, 1100 or 1300 °C, and M represents the meso-macroporous and monolithic properties of the composite material.

For comparison, Al_2O_3-1300-M was also prepared as reported in our previous paper [24].

2.2. Preparation of catalysts

Pt-Ni/5 wt.% CNT-Al_2O_3-1300-M catalysts were prepared by wet co-impregnation with aqueous solutions of $Pt(NH_3)_2(NO_3)_2$ and $Ni(NO_3)_2{\cdot}6H_2O$. After impregnation, the catalysts were frozen at 0 °C and stored at 0 °C for 12 h. They were subsequently freeze-dried for 12 h under vacuum for further use. The weight amounts of Pt and Ni in the catalyst, measured with ICP-AES, were 0.75 wt.% and 0.35 wt.%, respectively.

2.3. Characterization

Nitrogen adsorption and desorption isotherms were measured on a micromeritics apparatus (Tristar3000) at −196 °C. The specific surface areas were calculated using the BET method, and the pore size distributions were calculated from the desorption branch of the isotherms using the BJH model. All samples were outgassed under vacuum at 200 °C for 4 h prior to analysis.

The Pt and Ni content of the prepared catalysts were determined by inductively coupled plasma-atomic emission spectroscopy (ICP-AES, Vista-MPX, Varian).

X-ray diffraction (XRD) measurements were performed on a Bruker D8 Focus X-ray diffractometer with Ni-filtered Cu Kα radiation (λ = 0.15406 nm) at room temperature from 10.0° to 90.0° (scan rate = 5° min^{-1}).

Scanning electron microscopy (SEM) characterizations were performed on a Hitachi S4800 field-emission scanning electron microscope to observe the macroporous structures of the samples.

The morphologies of the catalysts were observed with transmission electron microscopy (TEM) on a Technai G^2 F20 microscope operated at 200 kV. Samples were pre-reduced at 300 °C in 62.5 vol.% H_2/N_2 for 2 h, finely ground to fine particles in a mortar and dispersed ultrasonically in ethanol. The well-dispersed samples were deposited onto a Cu gird covered by a porous carbon film for measurements.

The compressive strengths of the samples were measured using a Shimadzu DSS-25T universal testing machine. The samples were fixed with flat steel plates and closed with a circular head at a speed of 0.5 mm min^{-1}.

The thermal conductivity measurements were performed on XIATECH TC3010 thermal conductivity tester by the use of instantaneous heat ray method at room temperature.

2.4. Catalytic performance for CO-PROX

Catalytic performance tests were carried out on a continuous-flow fixed tubular reactor at atmospheric pressure. In each test, a piece of monolithic catalyst (6 mm length and 7 mm i.d.) was put into a temperature-resistant silicone tube, and the silicone tube was connected with two quartz tubes at both ends. Before the catalytic reaction, the as-dried catalyst was reduced at 300 °C for 2 h with 62.5 vol.% H_2 in N_2 at a heating rate of 10 °C min^{-1}. TPR results indicated that at this temperature nickel and platinum ions could be reduced to metallic form, for that the reduced platinum can catalyze the reduction of nickel ions [25]. The reaction mixture consisted of 1 vol.% CO, 1 vol.% O_2, 0–12.5 vol.% CO_2, 0–15 vol.% H_2O, and 50 vol.% H_2, with N_2 comprising the remainder of the balance. The total flow rate was 40 mL min^{-1}, corresponding to a volume space velocity of 10,400 h^{-1} and a mass space velocity of 24,000 mL g_{cat}^{-1} h^{-1}. The reaction temperature was monitored using a K-type thermocouple placed on the catalysts and was controlled with a temperature controller. The effluent gases were analyzed using an on-line gas chromatograph (GC, model SP-3420) equipped with a TCD and a column packed with 5 Å molecular sieves. An FID detector equipped with a methanator was used; thus, the CO detection limit was 1 ppm. The activities of the catalysts were evaluated on the basis of CO conversion. The selectivity of O_2 for CO oxidation was defined

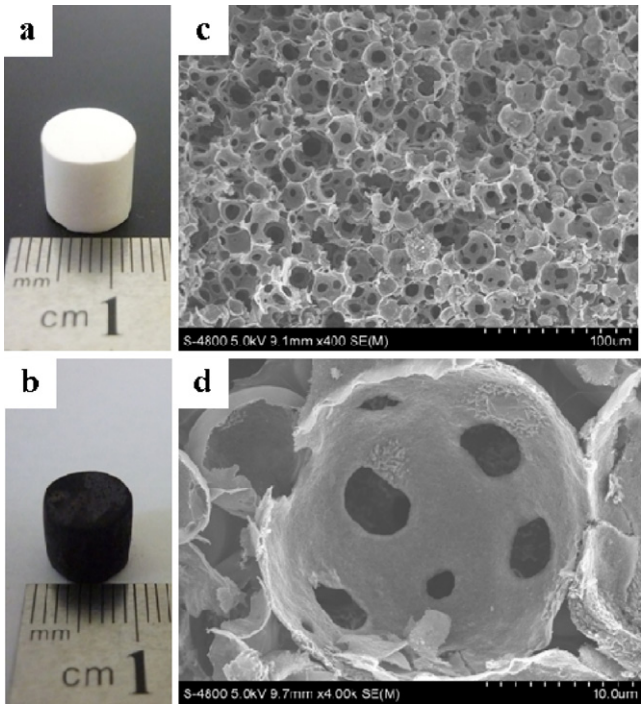

Fig. 1. Photographs of (a) PS template and (b) 15 wt.% CNT-Al_2O_3-1300-M; and SEM images of 15 wt.% CNT-Al_2O_3-1300-M with scale bars of (c) 100 μm and (d) 10 μm.

as the ratio of O_2 consumption used for CO oxidation to the total O_2 consumption. The equations are as follows:

$$\text{conversion of CO}(\%): X_{CO} = \frac{[CO]_{in} - [CO]_{out}}{[CO]_{in}} \times 100$$

$$\text{selectivity of } O_2 \text{ to CO}(\%): S_{O_2} = \frac{[CO]_{in} - [CO]_{out}}{2 \times ([O_2]_{in}) - [O_2]_{out}} \times 100$$

where $[CO]_{in}$ and $[O_2]_{in}$ are the concentration of CO and O_2, respectively, in the feed stream, and $[CO]_{out}$ and $[O]_{out}$ are the concentration of CO and O_2, respectively, in the effluent gases.

3. Results and discussion

3.1. Characterization of x wt.% CNT-Al_2O_3-y-M

3.1.1. Photographs and SEM images

Representative optical photographs of the PS template and 15 wt.% CNT-Al_2O_3-1300-M are shown in Fig. 1a and b. Monolithic CNT-Al_2O_3-1300-M composites were successfully prepared by imbibing PS templates with carbon nanotube-alumina hydrosols. The shapes of the CNT-alumina monoliths were almost identical to the PS templates, except that their size shrank to some degree. For the 15 wt.% CNT-Al_2O_3-1300-M, the volume shrank by approximately 38%.

The PS templates could be cut into various shapes with a knife, such as a cube, cylinder, or slice. In other words, the CNT-alumina monoliths could be formulated to any desired shape. Therefore, they should be convenient and flexible for nearly any application.

As shown in Fig. 1c and d and using 15 wt.% CNT-Al_2O_3-1300-M as an example, the macropores were spherical in shape with diameters ranging from 10 to 40 μm, which were interconnected through windows approximately 1–10 μm in size. The macroporous networks should be beneficial to mass transfer. The alumina matrix contained uniformly distributed carbon nanotubes, which are shown in Fig. 2f and f′.

Fig. 2 shows SEM images of the macropore walls of CNT-Al_2O_3-1300-M with varying amounts of CNTs sintered at 1300 °C. The Al_2O_3 grain size gradually decreased with increasing CNT content. At 0.5 wt.% CNTs, the grain size of the Al_2O_3 was essentially the same as pure alumina. However, the grain size of Al_2O_3 clearly decreased with an increase in CNT content (Fig. 2a–f). At 5 wt.% CNTs, the alumina grain size was less than 300 nm, which was much smaller than that of the monoliths containing 3 wt.% CNTs. Similar phenomena have previously been reported for MWNT/$BaTiO_3$ nanocomposite ceramics [26]. The reduction of grain size was ascribed to the pinning effect of the CNTs, which restricted the growth of the alumina grains [27]. As shown in Fig. 2, the CNTs projected out of the alumina body, and the amount of protruding increased as the CNT content increased.

At concentrations of CNTs of 3 wt.% or lower, the CNTs were uniformly and individually distributed throughout the composites (see Fig. 2b–d). When the CNT content was 5 wt.%, the CNTs still appeared to be distributed homogeneously throughout the alumina matrix (Fig. 2e, e′, g), although a few CNT bundles were formed. The uniform dispersion of the CNTs can also be seen from the cross-section of a pore in Fig. 2h. When the CNT content was increased to 15 wt.%, more CNTs and CNT bundles were observed in the pore walls, as shown in Fig. 2f. The porosities can be seen from the magnified image of Fig. 2f′. The highly distributed CNTs prevented the aggregation and sintering of the alumina grains, similar to what has previously been described in the literature [19].

SEM images of 5 wt.% CNT-Al_2O_3-y-M composite materials calcined at 600, 900 or 1100 °C are displayed in Fig. 3. For the sample that was calcined at 600 °C, it is noteworthy that the carbon nanotubes were mainly incorporated into the bulk of the Al_2O_3. Many obtuse tips of carbon nanotubes were uniformly dispersed throughout the composite surface, as indicated by the arrows in Fig. 3a. The diameters of the obtuse tips ranged from 10 to 20 nm, in accordance with the size of the carbon nanotubes. There were no holes surrounding the CNTs, indicating tight binding between the CNTs and Al_2O_3 matrix. As the calcination temperature increased to 900 °C and 1100 °C, the carbon nanotubes began protruding out of the Al_2O_3 matrix. Compared to the composite monoliths that were calcined at 1300 °C (Fig. 2e), the CNT protrusions of the monoliths that were calcined at 900 and 1100 °C were shorter and fewer in number.

In summary, in the meso-macroporous CNT-Al_2O_3 monoliths, the CNTs were uniformly distributed throughout the composite, and the alumina matrix was pinned by the CNTs into grains. Increasing calcination temperatures had little effect on the uniform distribution of the CNTs; however, it did make the aggregation of alumina more severe, resulting in CNTs protruding out of the Al_2O_3 matrix and the formation of pores between the CNTs and alumina grains.

As seen in the typical fracture surface shown in Fig. 3b′, it was interesting to find that some carbon nanotubes were perpendicular to the crack direction and bridged the cracked surfaces. The tight interfacial bindings between the CNTs and the Al_2O_3 assured a good stress transfer between the CNTs and the Al_2O_3 [28]. Therefore, it can be inferred that the presence of the CNTs improved the mechanical strength of the monoliths.

3.1.2. N_2 adsorption and desorption

Fig. 4 shows nitrogen adsorption–desorption isotherms and corresponding pore size distribution curves of the 5 wt.% CNT-Al_2O_3-y-M calcined at different temperatures and of the CNTs-OX. The adsorption parameters that were derived from these isotherms are summarized in Table 1. In all cases, except for the monoliths calcined at 1300 °C, the isotherms were classified as Type IV according to IUPAC definitions, which refer to mesoporous materials. The isotherms measured from the samples calcined at 600,

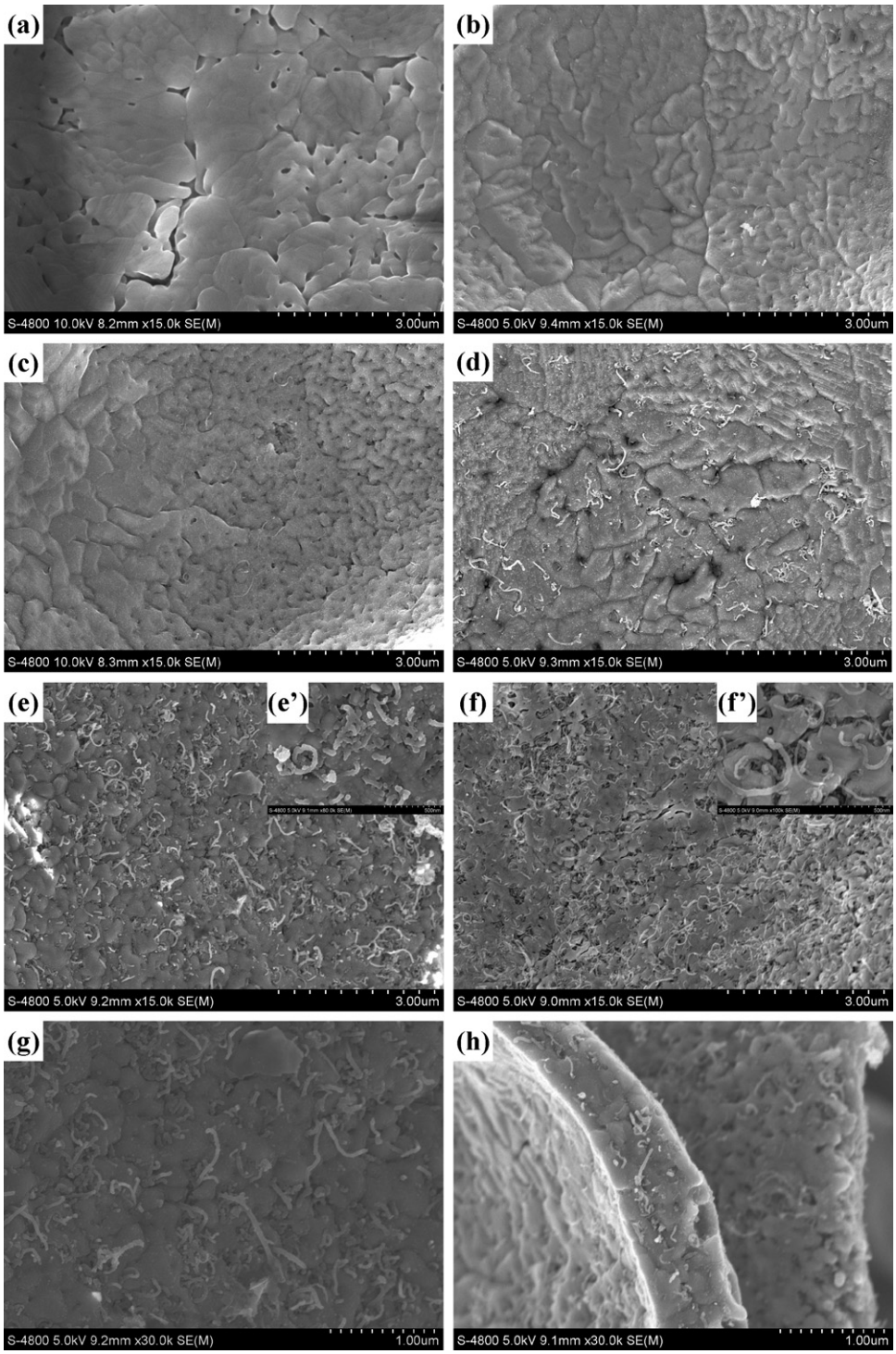

Fig. 2. SEM images of (a) Al_2O_3-1300-M, (b) 0.5 wt.% CNT-Al_2O_3-1300-M, (c) 1 wt.% CNT-Al_2O_3-1300-M, (d) 3 wt.% CNT-Al_2O_3-1300-M, (e, g, h, e′) 5 wt.% CNT-Al_2O_3-1300-M, (f and f′) 15 wt.% CNT-Al_2O_3-1300-M. Scale bars: 3 μm for (a–f), 1 μm for (g and h) and 500 nm for (e′, f′).

900 and 1100 °C exhibited H_1 hysteresis loops. For the sample calcined at 1300 °C, the isotherm was classified as type II, with an H_3-shape hysteresis loop. Moreover, the loops shifted to relatively high pressures as the calcination temperature increased, suggesting an increase in the size of the mesopores [29].

Shown in Fig. 4b, the CNTs displayed a broad pore size distribution from 2.5 to 70 nm, with a small peak near 4 nm and a broad peak ranging from 12 to 18 nm. The smaller mesopores were assigned to the inner pores of the CNTs, and the larger mesopores were due to the slits between the bundles of CNTs [30]. Narrow pore size distributions (3–6 nm) were observed for the monoliths calcined at 600 and 900 °C. Comparing the volume of nitrogen adsorbed near the mesopores in the size range of 3–6 nm between the pure CNTs and the composite monoliths, these mesopores were predominantly formed by the compacted alumina particles. Certainly, a small fraction of the mesopores was attributed to the inner pores of the carbon nanotubes. As the calcination temperature increased to 1100 °C, the average pore size increased to 6.4 nm due to the

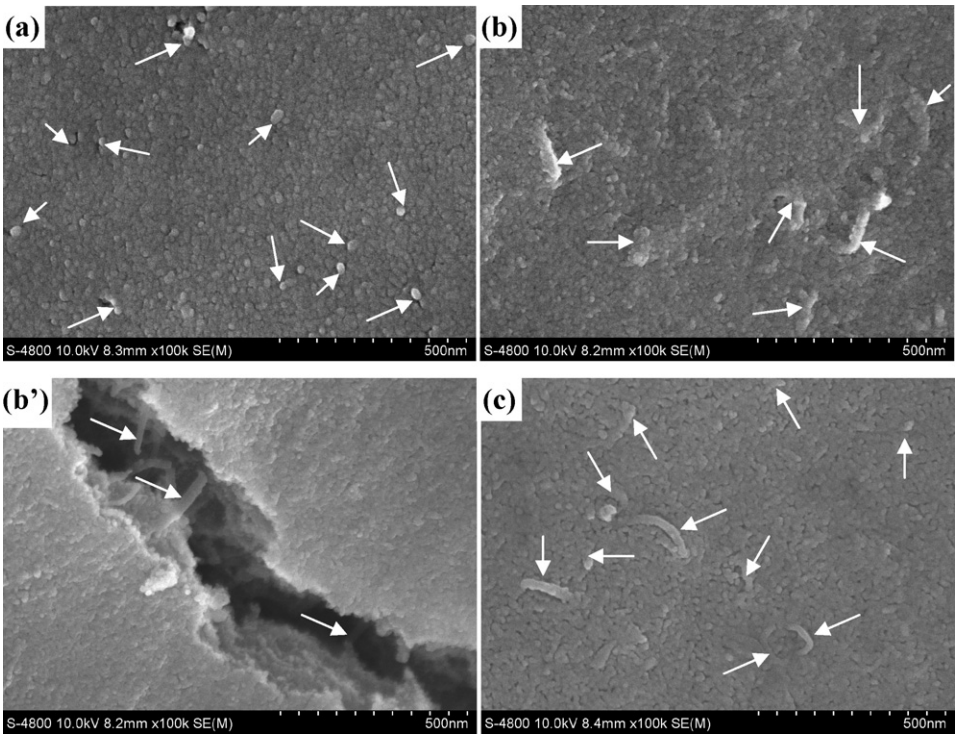

Fig. 3. SEM images of (a) 5 wt.% CNT-Al_2O_3-600-M, (b and b′) 5 wt.% CNT-Al_2O_3-900-M, (c) 5 wt.% CNT-Al_2O_3-1100-M. Arrows in images indicate carbon nanotubes. Scale bars: 500 nm.

sintering of the smaller mesopores. A small peak near 4 nm was still present, which was attributed to the inner pores of the carbon nanotubes. For the samples calcined at 600, 900 and 1100 °C, pores with size distributions above 10 nm were barely observed. This strongly suggested that there were no clusters of CNTs, i.e., the CNTs were distributed separately and uniformly throughout the composite monoliths, which was in good accord with the SEM images in Fig. 3. The mesopore size distributions of the composite monoliths mainly assumed those of the alumina. However, pores with size larger than 10 nm were present in monoliths calcined at 1300 °C, which will be discussed below.

The parameters that were derived from the adsorption of 5 wt.% CNT-Al_2O_3-*y*-M calcined at different temperatures are listed in Table 1. The BET surface areas and pore volumes dramatically decreased with increasing calcination temperature. A similar trend has previously been reported for pure alumina [24].

All of the nitrogen adsorption–desorption isotherms (Fig. 5) of the composite monoliths that were calcined at 1300 °C, regardless of the CNT content, were classified as type II, which is characteristic of macroporous materials. The H_3-shape hysteresis loops of each sample, except for pure alumina of Al_2O_3-1300-M, showed the presence of mesopores. The pore size distribution curve of the pure CNTs was reduced to 5% of its original value (Fig. 5b), which, based on the amount of CNTs, was equivalent to monoliths with 5 wt.% CNTs. Comparing the volumes of N_2 adsorbed in the mesopores that were approximately 4 nm, it was concluded that the mesopores were from the inner pores of the CNTs. For the monolith with 15 wt.% CNTs, some CNTs agglomerated together during preparation, leading to the formation of pores of approximately 10 nm in size, as described above for the mesopores of pure CNTs. During the high temperature calcination at 1300 °C, the sintering of the alumina was severe. This most likely resulted in the separation of the alumina particles and CNTs, which left behind interspaces. These interspaces produced the 10 nm mesopores for the monolithic composites calcined at 1300 °C. This can also be seen in Fig. 2f′ and Fig. 8b. Because of this porosity, even the composite monoliths that were calcined at 1300 °C still had high specific surface area, as shown in Table 1. As shown from the isotherm data in Table 1, the BET surface areas and pore volumes increased as the CNT content increased.

Table 1
Adsorption parameters, compressive strength and thermal conductivity of *x* wt.% CNT-Al_2O_3-*y*-M composite monoliths and CNTs-OX.

Sample	BET surface area ($m^2\ g^{-1}$)	Pore diameter (nm)	Pore volume ($cm^3\ g^{-1}$)	Compressive strength (MPa)	Thermal conductivity ($W\ m^{-1}\ K^{-1}$)[b]
CNTs-OX	108	12.5	0.40	–	–
Al_2O_3-1300-M	3	–	0.017	3.08	0.08468
0.5 wt.% CNT-Al_2O_3-1300-M	12	18.7	0.049	0.59	0.08624
1 wt.% CNT-Al_2O_3-1300-M	21	12.6	0.053	0.66	0.09535
3 wt.% CNT-Al_2O_3-1300-M	34	14.3	0.089	1.17	–
5 wt.% CNT-Al_2O_3-1300-M	48	12.5	0.128	1.89	0.1049
15 wt.% CNT-Al_2O_3-1300-M	80	9.1	0.163	1.23	0.08490
5 wt.% CNT-Al_2O_3-600-M	215	4.0	0.235	0.94 (0.123)[a]	0.08786
5 wt.% CNT-Al_2O_3-900-M	183	4.0	0.211	1.18 (0.713)[a]	–
5 wt.% CNT-Al_2O_3-1100–M	86	6.4	0.171	1.33 (0.759)[a]	–

[a] Data in parentheses are the compressive strength of pure alumina monolith calcined at the same temperature.
[b] The data of thermal conductivity are measured at room temperature.

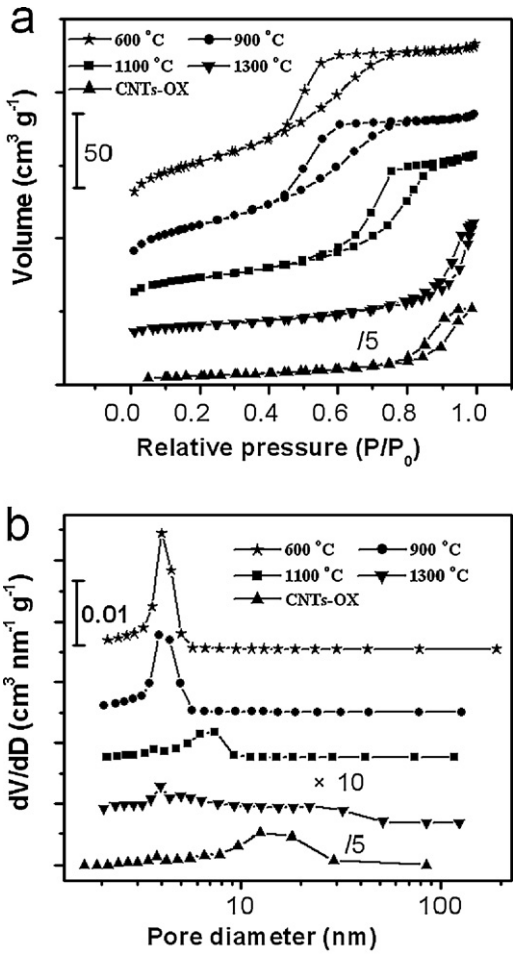

Fig. 4. (a) N_2 adsorption–desorption isotherms and (b) BJH pore size distribution curves of (⋆) 5 wt.% CNT-Al_2O_3-600-M, (●) 5 wt.% CNT-Al_2O_3-900-M, (■) 5 wt.% CNT-Al_2O_3-1100-M, (▼) 5 wt.% CNT-Al_2O_3-1300-M and (▲) CNTs-OX.

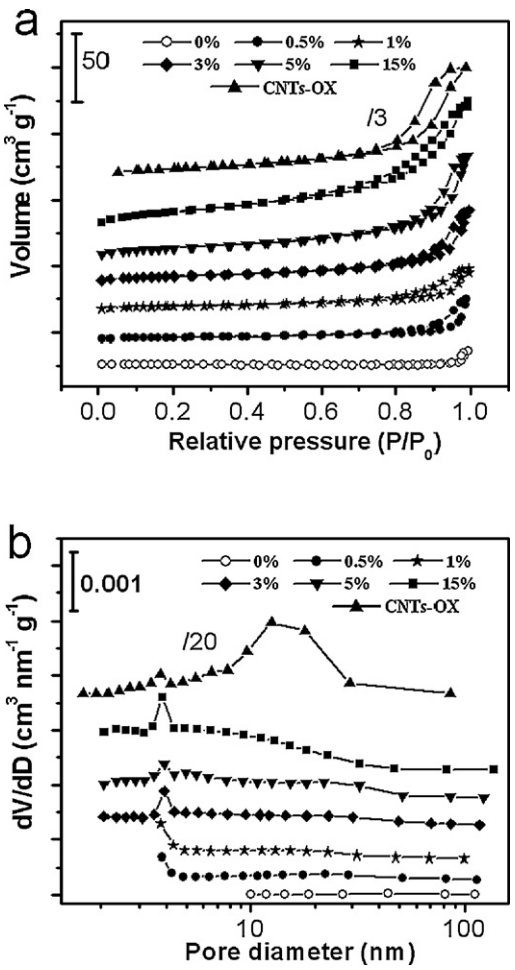

Fig. 5. (a) N_2 adsorption–desorption isotherms and (b) BJH pore size distribution curves of (○) Al_2O_3-1300-M, (●) 0.5 wt.% CNT-Al_2O_3-1300-M, (⋆) 1 wt.% CNT-Al_2O_3-1300-M, (♦) 3 wt.% CNT-Al_2O_3-1300-M, (▼) 5 wt.% CNT-Al_2O_3-1300-M, (■) 15 wt.% CNT-Al_2O_3-1300-M and (▲) CNTs-OX.

As mentioned above, the BET surface areas, pore volumes and pore sizes of the composite materials could be adjusted by modifying both the content of the CNTs and the calcination temperature.

To summarize this section, at calcination temperatures of 1100 °C or lower, mesopores of several nanometers were predominantly ascribed to the compacted alumina particles. As the calcination temperature was increased to 1300 °C, the mesopores from compacted alumina particles were sintered, and mesopores of approximately 10 nm in size were formed, which were the interspaces between the alumina matrix and the CNTs.

3.1.3. XRD patterns

Fig. 6 shows the XRD patterns of CNTs-OX and 5 wt.% CNT-Al_2O_3-*y*-M (*y* = 600, 900, or 1100 °C). The CNTs-OX exhibited two intense peaks at 26.5° and 43.3°, which were assigned to the (0 0 2) and (1 0 0) planes of the hexagonal graphite structure, respectively [31]. For 5 wt.% CNT-Al_2O_3-*y*-M (in Fig. 6b–d), the graphite signals at 26.5° were very weak due to the low CNT content in the composites. The structural phases of the composite monoliths calcined at 600 and 900 °C were γ-Al_2O_3, but at a calcination temperature of 1100 °C, the phase was θ-Al_2O_3. This agreed with the pure Al_2O_3 that was calcined at the same temperature [24], indicating that the presence of the CNTs in the composite monoliths did not significantly affect the crystal phase transition of Al_2O_3.

The XRD patterns of *x* wt.% CNT-Al_2O_3-1300-M (*x* = 0.5, 1, 3, 5, or 15) and Al_2O_3-1300-M are shown in Fig. 7. For all of the composite monoliths calcined at 1300 °C, the sharp diffraction peaks of the α-Al_2O_3 phase (JCPDS Card No. 46-1212) appeared, indicating that the concentration of CNTs did not influence the crystal phase of Al_2O_3 at all. The peaks corresponding to CNTs were very weak due to the good crystallization of the Al_2O_3 particles and the relatively low CNT content.

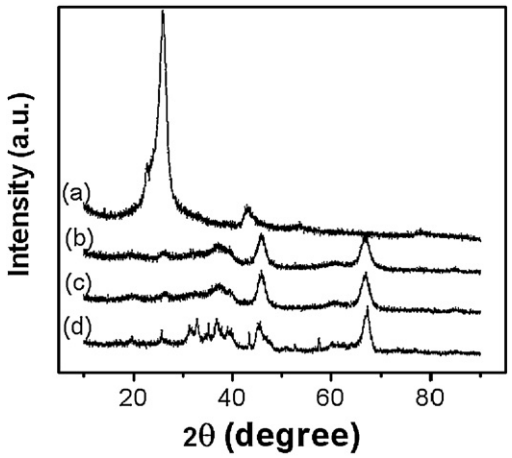

Fig. 6. XRD patterns of (a) CNTs-OX, (b) 5 wt.% CNT-Al_2O_3-600-M, (c) 5 wt.% CNT-Al_2O_3-900-M, and (d) 5 wt.% CNT-Al_2O_3-1100-M.

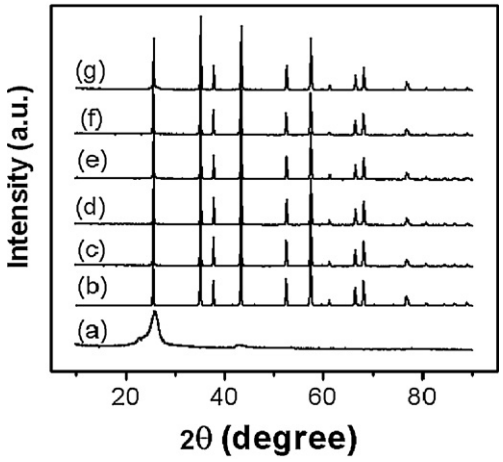

Fig. 7. XRD patterns of (a) CNTs-OX, (b) Al_2O_3-1300-M, (c) 0.5% CNT-Al_2O_3-1300-M, (d) 1 wt.% CNT-Al_2O_3-1300-M, (e) 3 wt.% CNT-Al_2O_3-1300-M, (f) 5 wt.% CNT-Al_2O_3-1300-M and (g) 15 wt.% CNT-Al_2O_3-1300-M.

3.1.4. Mechanical properties and thermal conductivity

As shown in Table 1, the compressive strength of the monolithic composites was highly dependent on the CNT content and calcination temperature. For the monoliths calcined at 1300 °C, increasing the CNT content from 0.5 to 5 wt.% resulted in a strength increase from 0.59 to 1.89 MPa. It then decreased to 1.23 MPa as the CNT content was increased to 15 wt.%. For the monoliths containing high concentrations of CNTs, the comparatively poor mechanical strength was likely due to the high degree of porosity, similar to CNT-alumina ceramic powders, as has previously been reported [19].

At concentrations of CNT fixed at 5 wt.%, the compressive strength of the monoliths increased with increasing calcination temperature. For example, the composite material showed a compressive strength of 0.94 MPa after calcination at 600 °C and 1.89 MPa after calcination at 1300 °C.

Comparing the pure alumina monoliths and the CNT-alumina composites at calcination temperatures of 1100 °C or less, an addition of 5 wt.% CNTs to the macroporous monolithic alumina led to an increase in the compressive strength. For example, the compressive strength of 5 wt.% CNT-Al_2O_3-600-M was nearly eight times greater than that of the Al_2O_3-600-M. At a calcination temperature of 1300 °C, the compressive strength of all the CNT-alumina monoliths was lower than that of pure alumina.

After combining the results of the mesopore formation mechanisms ascribed from the N_2 isotherms with the SEM images, the following conclusions were obtained with regard to the mechanical strength of the composite monolith. CNTs in the monoliths elevated the mechanical strength of the composite monoliths, as shown in Fig. 3b. However, the porosity resulting from the addition of the CNTs lowered the mechanical strength of the composite monoliths. At the high calcination temperature of 1300 °C, some CNTs were separated from the alumina matrix and left behind mesopores, leading to poorer mechanical strength than the pure alumina monolith. At calcination temperatures of 1100 °C or less and a CNT content equal to or less than 5 wt.%, CNTs bound well with alumina and were uniformly and individually dispersed. Therefore, the addition of CNTs into the monoliths improved their mechanical strength.

Thermal conductivity of the monoliths is shown in Table 1. It can be seen that the CNTs content and calcination temperature influenced the thermal conductivity markedly. For the monoliths calcined at 1300 °C, the thermal conductivity increased with the CNTs content increased from none to 5 wt.%. When 5 wt.% CNTs was incorporated into the pure alumina monolith, a 24% increase of the thermal conductivity is observed compared with the pure Al_2O_3 monolith. However, as CNTs content further increased to 15 wt.%, the thermal conductivity decreased, which is close to that of the pure alumina monolith. The relatively poor thermal conductivity of 15 wt.% CNTs-Al_2O_3 monolith should be due to the enriched pores among the alumina matrix, which compromise the thermal conductivity by scattering the heat flow.

The thermal conductivity increased with the increase of calcination temperature. As for the samples of CNT content fixed at 5 wt.%, the thermal conductivity is 0.08786 W m^{-1} K^{-1} for the sample calcined at 600 °C and it is 0.1049 W m^{-1} K^{-1} for the sample calcined at 1300 °C, with a increase of 19%. This is consistent with the results observed for other carbon nanotubes-alumina ceramic composites [32]. The high calcination temperature results in the increase of alumina grain size and reduction of pores, leading to the increase of thermal conductivity [33].

In conclusion, the thermal conductivity of the composite monoliths can be improved with adding appropriate amounts of CNTs and with suitable calcination temperature.

3.1.5. TEM images of the 0.75 wt.% Pt/0.35 wt.% Ni/5 wt.% CNT-Al_2O_3-1300-M catalyst

From the TEM images in Fig. 8a and b, it was evident that the alumina nanoparticles sintered together. Some carbon nanotubes protruded from the alumina matrix, and some were distributed in the bulk of the alumina grains. It is interesting to note that interspaces were present between the carbon nanotubes and the alumina grains in some locations, as indicated by the arrow in Fig. 8b. This was consistent with the SEM images (Fig. 2).

Platinum and nickel nanoparticles were dispersed uniformly throughout the carbon nanotubes and alumina, as displayed in Fig. 8c and d. The average particle size was approximately 2 nm. The active nanoparticles preferred to anchor onto the carbon nanotubes rather than the alumina, which was ascribed to the higher surface area of the CNTs. The mechanism of active component deposition on carbon nanotubes or alumina requires further study.

3.1.6. Catalytic performance of the 0.75 wt.% Pt/0.35 wt.% Ni/5 wt.% CNT-Al_2O_3-1300-M catalyst

The conversion of CO and the selectivity of O_2 to CO oxidation with reaction temperature in a 5 wt.% CNT-Al_2O_3-1300-M-supported Pt-Ni catalyst are presented in Fig. 9. The effects of H_2O and CO_2 on the catalytic performance are also shown. CO was purified completely at 100–150 °C in gases consisting of 1 vol.% CO, 1 vol.% O_2, 50 vol.% H_2 and 48 vol.% N_2 with a volume space velocity of 10,400 h^{-1}. The selectivity of O_2 to CO oxidation was approximately 51.5%. As the reaction temperature increased to 175 °C, the CO conversion decreased to 98.9% with a CO selectivity of 49.9% due to the competing reaction of H_2 oxidation [34,35]. Similar behaviors have been reported for supported platinum catalysts [8,36]. On the whole, the monoliths exhibited excellent activity and selectivity.

Upon the addition of 12.5 vol.% CO_2 to the feed gases, a 100% conversion of CO was achieved in the temperature range from 100 to 125 °C, and the selectivity of O_2 to CO oxidation was maintained at 51.0%. At 150 °C, the conversion of CO dropped to 99.95% with 49.7% selectivity, which corresponded to 5 ppm of the residual concentration of CO. Therefore, the CO_2 had a slight influence on CO purification using this composite monolithic catalyst.

The addition of 15 vol.% H_2O into the feed decreased the CO conversion from 100% to 93.9% at 100 °C. The maximum conversion of CO was 99.70% at 120 °C, and the corresponding concentration of the residual CO was 30 ppm. The conversion of CO at 140 °C and 160 °C were 99.60% and 99.16%, corresponding to 40 and 84 ppm

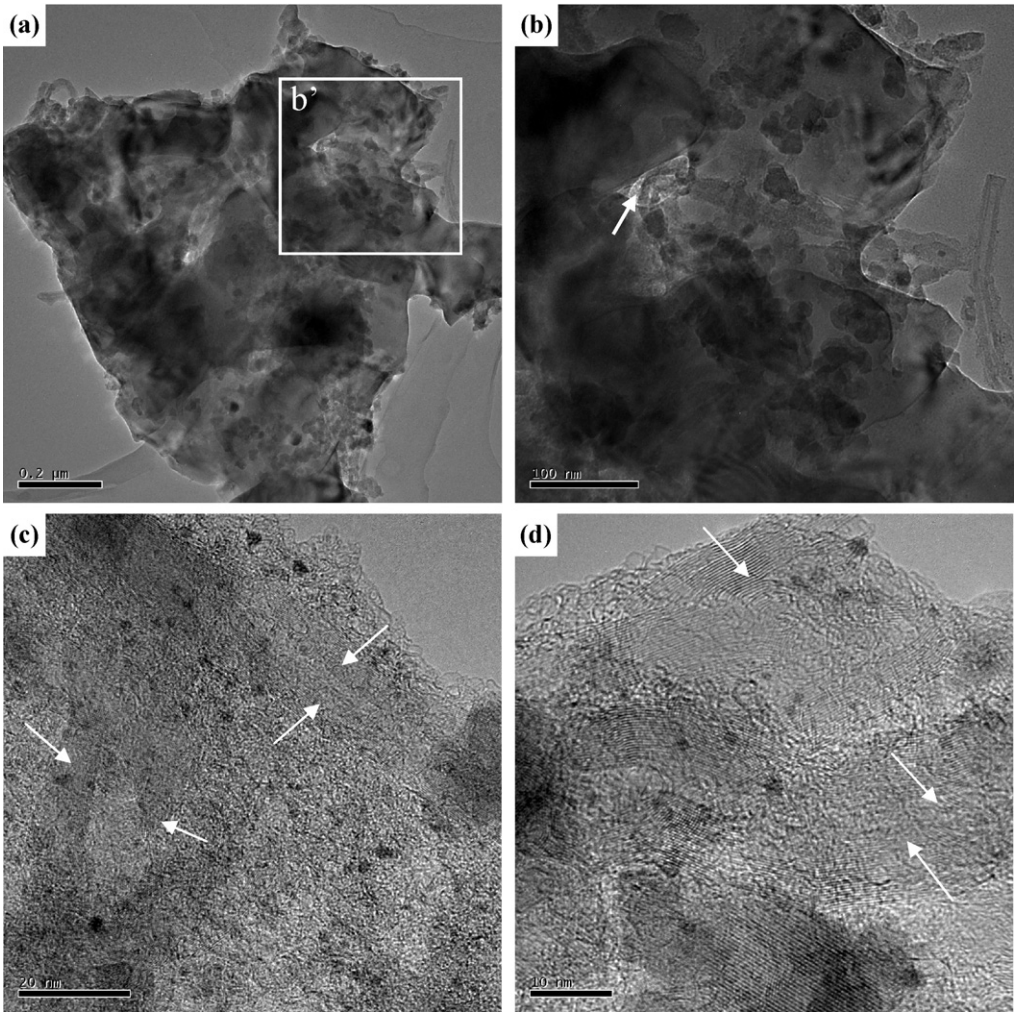

Fig. 8. TEM images of 0.75 wt.% Pt/0.35 wt.% Ni/5 wt.% CNT-Al_2O_3-1300-M with scale bars of (a) 0.2 μm, (b) 100 nm, (c) 20 nm and (d) 10 nm. (b) is the magnified view of (b′). Arrows in images of (c and d) indicate carbon nanotubes.

of exit CO concentration, respectively. The selectivity of O_2 to CO remained at 50.0%. The effect of water was therefore more severe than that of CO_2.

Upon the addition of both 12.5 vol.% CO_2 and 15 vol.% H_2O, CO was still purified to lower than 100 ppm in the temperature range of 120–180 °C, although the CO purification efficiency further decreased slightly at the low temperature of 100 °C. The highest attainable CO conversion was approximately 99.64% at 120 °C with 50.7% selectivity. At a reaction temperature of 180 °C, the residual concentration of CO was 94 ppm, and the selectivity of O_2 to CO oxidation was 49.9%. The composite monolithic catalyst displayed excellent catalytic performance for CO-PROX.

The variation of CO conversion and the selectivity of O_2 to CO oxidation with reaction time on stream are shown in Fig. 10. 100% CO conversion and 51.1% selectivity of O_2 to CO oxidation were obtained for 15 h at 120 °C in reaction gas of 1 vol.% CO, 1 vol.% O_2, 50 vol.% H_2 and N_2 balance. When 12.5 vol.% CO_2 and 15 vol.% H_2O were added, the CO conversion and the selectivity decreased slightly to 99.64% and 50.9%, respectively. After 23 h running, CO conversion further dropped a little close to 99.0%, corresponding to 100 ppm of CO in the exit gases. To elevate the reaction temperature to 130 °C, 99.64% of CO conversion was recovered and maintained for 25 h. Then the CO conversion dropped a little too. To elevate the reaction temperature to 140 °C, CO was purified to less than 100 ppm in the following 18 h. In the 80 h running period, CO was purified to less than 100 ppm. However, improvement for the catalyst stability is needed.

It has been reported that the presence of CO_2 in the feed has a detrimental effect on the activity of Al_2O_3 supported Pt catalyst [37], due to a partial coverage of active sites by CO_2. For Pt-Ni/CNTs-Al_2O_3-M catalyst, CO_2 has a slight negative influence of on the catalyst activity. The good resistance of Pt-Ni/CNTs-Al_2O_3-1300-M to CO_2 may be attributed to surface oxygen bearing groups on CNTs-OX, such as hydroxyl and carboxyl. When carboxyl groups decompose into CO_2, free carbon atoms can be generated at the carbon nanotubes layer, which will reversibly adsorb surface CO_2 [38]. The mobile oxygen blocked by CO_2 or dissociation of CO_2 on the metallic sites may be avoided [35].

For supported Pt catalysts, it has been reported that the catalyst activity may be slightly enhanced by the addition of water [35,39]. Manasilp and co-workers pointed out that the enhancement of water was due to the participation of the hydroxyl groups formed by the dissociative adsorption of H_2O on Pt. However, for Pt-Ni/CNTs-Al_2O_3-M, at 100 °C the presence of water in the feed has a negative effect on CO conversion, which may be due to the capillary wetting of water in the mesopores of the carbon nanotubes [23]. At the high temperatures of 175 and 200 °C, the water apparently had no negative effect on CO conversion, as shown in Fig. 9. This was most likely due to the disappearance of the water at

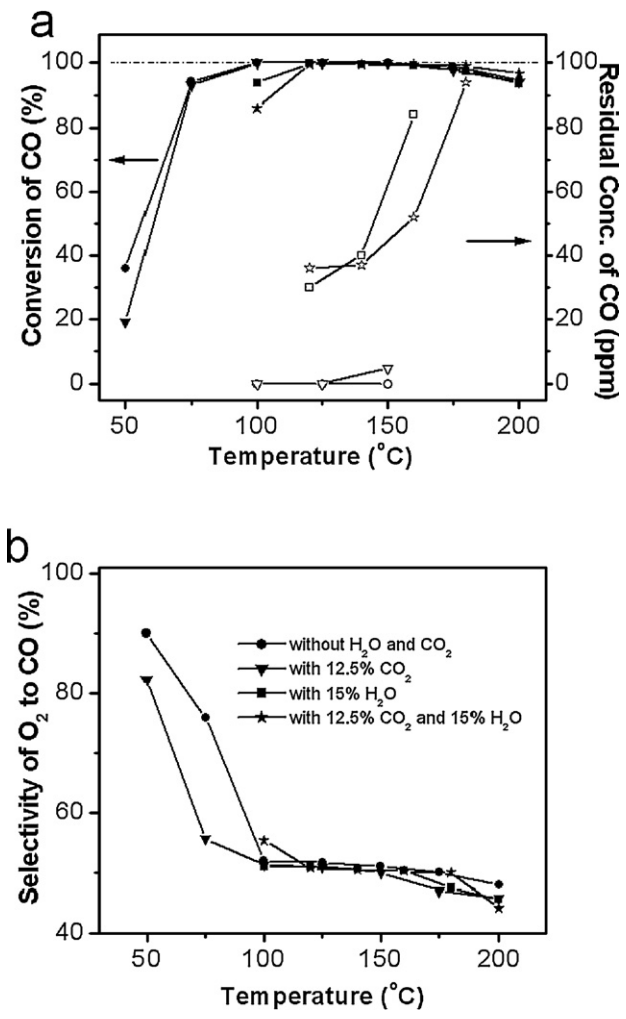

Fig. 9. Reaction temperature dependence of (a) CO conversion (filled symbol) and residual concentration of CO (open symbol), (b) the selectivity of O_2 to CO oxidation over 0.75 wt.% Pt/0.35 wt.% Ni/5 wt.% CNT-Al_2O_3-1300-M catalyst for CO-PROX. Reaction conditions: 1 vol.% CO, 1 vol.% O_2, 0–12.5 vol.% CO_2, 0–15 vol.% H_2O, 50 vol.% H_2 and N_2 (balance) for (●, ○) 0 vol.% CO_2 and 0 vol.% H_2O, (▼, ▽) 12.5 vol.% CO_2, (■, □) 15 vol.% H_2O, and (★, ☆) 12.5 vol.% CO_2 and 15 vol.% H_2O.

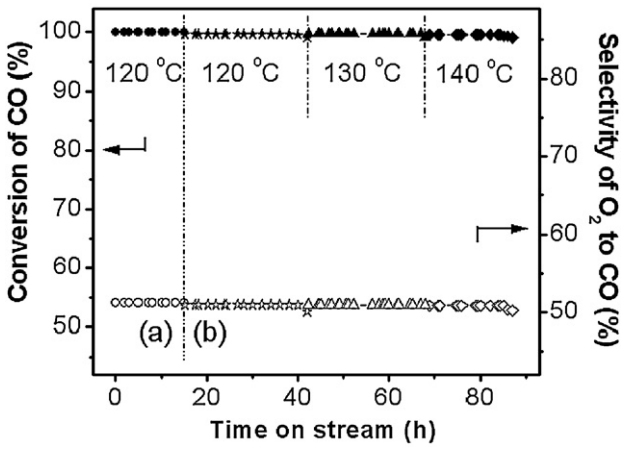

Fig. 10. Variation of CO conversion (filled symbol) and the selectivity of O_2 to CO oxidation (open symbol) with time on stream over 0.75 wt.% Pt/0.35 wt.% Ni/5 wt.% CNT-Al_2O_3-1300-M catalyst for CO-PROX. (a) 1 vol.% CO, 1 vol.% O_2, 50 vol.% H_2 and N_2 (balance), (b) 1 vol.% CO, 1 vol.% O_2, 12.5 vol.% CO_2, 15 vol.% H_2O, 50 vol.% H_2 and N_2 (balance). The volume space velocity is 10,400 h^{-1}.

the high temperatures and the contribution of the water–gas shift reaction.

The excellent catalytic performance of 0.75 wt.% Pt/0.35 wt.% Ni/5 wt.% CNT-Al_2O_3-1300-M was due, in part, to the high thermal conductivity of the CNTs, which allow the catalysts to avoid hotspot formations. Thus, the reverse WGS reaction, which is endothermic, can effectively be depressed.

Pt-Ni/CNTs-Al_2O_3-M catalyst can remove CO to under 100 ppm at much higher volume space velocity, in comparison with other monolithic catalysts [40,41]. This catalyst can be made to a piece or other wanted shape. CO can be purified when hydrogen gases pass through the piece. Potentially, this monolithic catalyst can be used in compact or miniaturized hydrogen production system.

4. Conclusions

Imbibing macroporous monolithic polystyrene foams with carbon nanotube-alumina hydrosols was a practical and highly efficient synthetic method for the preparation of meso-macroporous carbon nanotube-alumina monoliths. These prepared composite materials possessed interconnected spherical macropores, adjusted mesopores, and a monolithic framework in which carbon nanotubes were distributed uniformly throughout the alumina matrix. The macroporous monolithic structure was due to the PS template. The mesopores, mechanical properties and thermal conductivity of these monoliths were significantly influenced by the CNT content and calcination temperature. However, the phase transitions of Al_2O_3 at different temperatures were not affected by the addition of CNTs. The catalyst constructed from 0.75 wt.% Pt/0.35 wt.% Ni/CNT-Al_2O_3 monolith calcined at 1300 °C showed high activity and selectivity for the PROX of CO in H_2-rich gases. These monolithic composite materials should offer great potential for use in a wide range of applications, including catalytic, sensing, electronic and medical applications. The preparation method for monolithic CNT-alumina composites should be applicable to other CNT-metal oxide monoliths.

Acknowledgement

Financial support for this work was provided by the NSF of China (no. 20976121) is gratefully acknowledged.

References

[1] E.D. Park, D. Lee, H.C. Lee, Catal. Today 139 (2009) 280–290.
[2] N. Bion, F. Epron, M. Moreño, F. Mariio, D. Duprez, Top. Catal. 51 (2008) 76–88.
[3] E.Y. Ko, E.D. Park, K.W. Seo, H.C. Lee, D. Lee, S. Kim, Catal. Lett. 110 (2006) 275–279.
[4] E.Y. Ko, E.D. Park, H.C. Lee, D. Lee, S. Kim, Angew. Chem. Int. Ed. 46 (2007) 734–737.
[5] O. Pozdnyakova-Tellinger, D. Teschner, J. Krŏhnert, F.C. Jentoft, A. Knop-Gericke, R. Schlăgl, A. Wootsch, J. Phys. Chem. C 111 (2007) 5426–5431.
[6] A. de Lucas-Consuegra, A. Princivalle, A. Caravaca, F. Dorado, C. Guizard, J.L. Valverde, P. Vernoux, Appl. Catal. B: Environ. 94 (2010) 281–287.
[7] M. Kipnis, E. Volnina, Appl. Catal. B: Environ. 98 (2010) 193–203.
[8] S.K. Jain, E.M. Crabb, L.E. Smart, D. Thompsett, A.M. Steele, Appl. Catal. B: Environ. 89 (2009) 349–355.
[9] T. Ebashi, Y. Ishida, Y. Nakagawa, S.I. Ito, T. Kubota, K. Tomishige, J. Phys. Chem. C 114 (2010) 6518–6526.
[10] I. Rosso, C. Galletti, G. Saracco, E. Garrone, V. Specchia, Appl. Catal. B: Environ. 48 (2004) 195–203.
[11] B.S. Caglayan, İ.I. Soykal, A.E. Aksoylu, Appl. Catal. B: Environ. 106 (2011) 540–549.
[12] E. Castillejos, R. Chico, R. Bacsa, S. Coco, P. Espinet, M. Pérez-Cadenas, A. Guerrero-Ruiz, I. Rodríguez-Ramos, P. Serp, Eur. J. Inorg. Chem. 32 (2010) 5096–5102.
[13] K.I. Tanaka, M. Shou, Y.Z. Yuan, J. Phys. Chem. C 114 (2010) 16917–16923.
[14] J.P. Dacquin, J. Dhainaut, D. Duprez, S. Royer, A.F. Lee, K. Wilson, J. Am. Chem. Soc. 131 (2009) 12896–12897.
[15] M. Etienne, S. Sallard, M. Schrŏder, Y. Guillemin, S. Mascotto, B.M. Smarsly, A. Walcarius, Chem. Mater. 22 (2010) 3426–3432.
[16] P. Innocenzi, L. Malfatti, G.J.A.A. Soler-Illia, Chem. Mater. 23 (2011) 2501–2509.

[17] M. Crippa, E. Callone, M. D'Arienzo, K. Müller, S. Polizzi, L. Wahba, F. Morazzoni, R. Scotti, Appl. Catal. B: Environ. 104 (2011) 282–290.
[18] M.A. Worsley, S.O. Kucheyev, J.D. Kuntz, T.Y. Olson, T.Y.J. Han, A.V. Hamza, J.H. Satcher Jr., T.F. Baumann, Chem. Mater. 23 (2011) 3054–3061.
[19] T. Zhang, L. Kumari, G.H. Du, W.Z. Li, Q.W. Wang, K. Balani, A. Agarwal, Compos. Part A 40 (2009) 86–93.
[20] P.F. Fulvio, P.I. Brosey, M. Jaroniec, ACS Appl. Mater. Interfaces 2 (2010) 588–593.
[21] J.P. Daccquin, J. Dhainaut, D. Duprez, S. Royer, A.F. Lee, K. Wilson, J. Am. Chem. Soc. 131 (2009) 12896–12897.
[22] L.L. Li, W.T. Duan, Q. Yuan, Z.X. Li, H.H. Duan, C.H. Yan, Chem. Commun. 41 (2009) 6174–6176.
[23] S.H. Lu, C. Zhang, Y. Liu, Int. J. Hydrogen Energy 36 (2011) 1939–1948.
[24] Y. Zhang, H. Liang, C.Y. Zhao, Y. Liu, J. Mater. Sci. 44 (2009) 931–938.
[25] B.T. Li, S. Kado, Y. Mukainakano, T. Miyazawa, T. Miyao, S. Naito, K. Okumura, K. Kunimori, K. Tomishige, J. Catal. 245 (2007) 144–155.
[26] Q. Huang, L. Gao, J. Mater. Chem. 14 (2004) 2536–2541.
[27] S.C. Zhang, W.G. Fahrenholtz, G.E. Hilmas, E.J. Yadlowsky, J. Eur. Ceram. Soc. 30 (2010) 1373–1380.
[28] J. Sun, L. Gao, W. Li, Chem. Mater. 14 (2002) 5169–5172.
[29] W.Q. Cai, J.G. Yu, C. Anand, A. Vinu, M. Jaroniec, Chem. Mater. 23 (2011) 1147–1157.
[30] D.Y. Kim, C.M. Yang, Y.S. Park, K.K. Kim, S.Y. Jeong, J.H. Han, Y.H. Lee, Chem. Phys. Lett. 413 (2005) 135–141.
[31] H. Ismaili, F. Laguguné-Labarthet, M.S. Workentin, Chem. Mater. 23 (2011) 1519–1525.
[32] L. Kumari, T. Zhang, G.H. Du, W.Z. Li, Q.W. Wang, A. Datye, K.H. Wu, Compos. Sci. Technol. 68 (2008) 2178–2183.
[33] R. Sivakumar, S. Guo, T. Nishimura, Y. Kagawa, Scripta Mater. 56 (2007) 265–268.
[34] X. Ouyang, L. Bednarova, P. Ho, R.S. Besser, AIChE J. 51 (2005) 1758–1768.
[35] A. Manasilp, E. Gulari, Appl. Catal. B: Environ. 37 (2002) 17–25.
[36] M.M.V.M. Souz, N.F.P. Ribeiro, M. Schmal, Int. J. Hydrogen Energy 32 (2007) 425–429.
[37] J.L. Ayastuy, M.P. González-Marcos, J.R. González-Velasco, M.A. Gutiérrez-Ortiz, Appl. Catal. B: Environ. 70 (2007) 532–541.
[38] E. Şimsek, Ş. Özkara, A.E. Aksoylu, Z.I. Önsan, Appl. Catal. A: Gen. 316 (2007) 169–174.
[39] Y.F. Han, M.J. Kahlich, M. Kinne, R.J. Behm, Appl. Catal. B: Environ. 50 (2004) 209–218.
[40] C. Galletti, S. Specchia, G. Saracco, V. Specchia, Chem. Eng. J. 154 (2009) 246–250.
[41] N. Maeda, T. Matsushima, M. Kotobuki, T. Miyao, H. Uchida, H. Yamashita, M. Watanabe, Appl. Catal. A: Gen. 370 (2009) 50–53.